

An actively controlled silicon ring resonator with a fully tunable Fano resonance

A. Li, and W. Bogaerts

Citation: [APL Photonics](#) **2**, 096101 (2017);

View online: <https://doi.org/10.1063/1.5000514>

View Table of Contents: <http://aip.scitation.org/toc/app/2/9>

Published by the [American Institute of Physics](#)

Articles you may be interested in

[Split-disk micro-lasers: Tunable whispering gallery mode cavities](#)

[APL Photonics](#) **2**, 096103 (2017); 10.1063/1.4985766

[Integrating cell on chip—Novel waveguide platform employing ultra-long optical paths](#)

[APL Photonics](#) **2**, 096102 (2017); 10.1063/1.5001486

[Recommendations and illustrations for the evaluation of photonic random number generators](#)

[APL Photonics](#) **2**, 090901 (2017); 10.1063/1.5000056

[Reconfigurable broadband microwave photonic intensity differentiator based on an integrated optical frequency comb source](#)

[APL Photonics](#) **2**, 096104 (2017); 10.1063/1.4989871

[Ultra-high Q/V hybrid cavity for strong light-matter interaction](#)

[APL Photonics](#) **2**, 086101 (2017); 10.1063/1.4994056

[Micro-ring resonator quality factor enhancement via an integrated Fabry-Perot cavity](#)

[APL Photonics](#) **2**, 056103 (2017); 10.1063/1.4981392



STEM CAREER WEBINARS

on networking, interviewing, conferences, presenting...

www.physicstoday.org/jobs/webinars

AIP American Institute of Physics

The banner features a series of colorful speech bubbles containing icons for a microscope, a graduation cap, an atom, a test tube rack, and a flask. The AIP logo is prominently displayed in a green bubble on the left.

An actively controlled silicon ring resonator with a fully tunable Fano resonance

A. Li^{1,2,a} and W. Bogaerts²

¹Department of Information Technology, Photonics Research Group, Ghent University-IMEC, 9052 Ghent, Belgium

²Center for Nano- and Biophotonics, Ghent University, 9052 Ghent, Belgium

(Received 27 March 2017; accepted 13 August 2017; published online 29 August 2017)

We demonstrate a novel way to generate Fano resonance with tunable wavelength, extinction ratio, and slope rate. The device is a silicon add-drop microring with two integrated tunable reflectors inside, which form an embedded Fabry-Perot cavity. The fabrication is executed at a commercial CMOS foundry. Fano resonance at the drop port is generated from the interference between the Fabry-Perot cavity mode and the ring resonance mode. By tuning the reflectivities of these two reflectors with integrated heaters, various Fano resonance shapes can be achieved with a maximum extinction ratio over 40 dB and a slope rate more than 700 dB/nm. © 2017 Author(s). All article content, except where otherwise noted, is licensed under a Creative Commons Attribution (CC BY) license (<http://creativecommons.org/licenses/by/4.0/>). [<http://dx.doi.org/10.1063/1.5000514>]

Fano resonance originates from the interference between a continuous background mode and a discrete resonant mode and has attracted strong research interest since it was first proposed by Fano.¹ Its extremely sharp slope and asymmetric shape facilitate high-efficiency sensors, ultra-fast and low-power consumption switches and modulators, ultra small laser cavities, and slow-light applications.^{2–6}

For many of those applications, it is either necessary or highly desirable for use as photonics integrated circuits. Indeed, Fano resonances have already been demonstrated in integrated optics through various approaches.^{7–12} Unfortunately each of these methods has its drawbacks; either the devices are not fully integrated or they suffer from a relatively low extinction ratio (ER) and slope rate as well as poor tunability. Our approach, on the other hand, relies on a fully integrated circuit on a silicon-on-insulator (SOI) substrate that has a very small footprint and can be manufactured at a large scale with low cost. Moreover, it provides efficient tunability with a maximum ER over 40 dB and a slope sharper than 700 dB/nm, which—to our best knowledge—are the largest values realized so far. The device consists of a ring resonator and two integrated tunable reflectors inside, as shown in Figs. 1(a) and 1(c). These two reflectors form an embedded Fabry-Perot cavity [illustrated in Figs. 1(b) and 1(d)] which generates a slowly varying background mode that interferes with the discrete ring resonances at the drop port of the ring resonator. The resulting Fano resonance can be easily tuned by controlling the reflectivities of the two reflectors which determine the Fabry-Perot mode.

Fan theoretically proposed a similar approach, where two partially transmitting elements at the bus waveguide were used to form a Fabry-Perot cavity outside the ring cavity.¹⁴ Zhang *et al.* made an experimental implementation of the structure proposed by Fan in a silicon photonics platform,¹⁰ where they used two sidewall gratings as the partially transmitting elements. However, the parameters of the Fabry-Perot cavity (grating period, cavity length, etc.) formed by those sidewall gratings, which determine the properties of the Fano resonance, can only be physically adjusted instead of dynamically tuned. Thus they can only achieve tuning of the Fano resonance by injecting a high power pump laser to optically modify the coupling strength between the Fabry-Perot cavity and the ring cavity. This

^aElectronic mail: ang.li@ugent.be

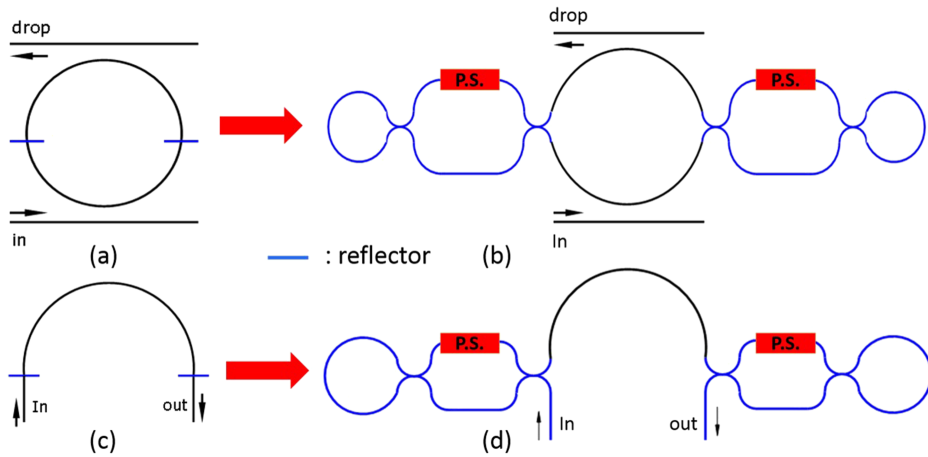


FIG. 1. (a) and (c) give conceptual illustrations of our device and the Fabry-Perot cavity formed by two reflectors, which are represented by blue lines. (b) and (d) show the schematics where the loop-ended MZI based reflectors replace the blue lines.

is impractical for many applications and has a poor tuning range and efficiency. The maximum ER and slope rate reported is limited to 22.54 dB and 250.4 dB/nm, respectively.

As shown in Fig. 1, the tunable reflector itself is a small sub-circuit based on a Mach-Zehnder-Interferometer (MZI) whose two outputs are connected. By controlling the phase shift of one arm of the MZI over π radians, the reflectivity can be tuned from 0% to almost 100%, as shown in Fig. 2(a). Note that the starting point of the reflector in our simulated device is not 0 as we choose the directional couplers not to operate as 50/50 splitter. This reflects the reality of the fabrication variation because the splitting ratio of directional couplers may deviate from 50/50. More details about the reflector can be found in Ref. 15. In Figs. 2(b)–2(e), we plot the simulated spectra of the Fabry-Perot cavity as well as the complete device. The simulations are performed in the optical circuit simulator *Caphe* by Luceda

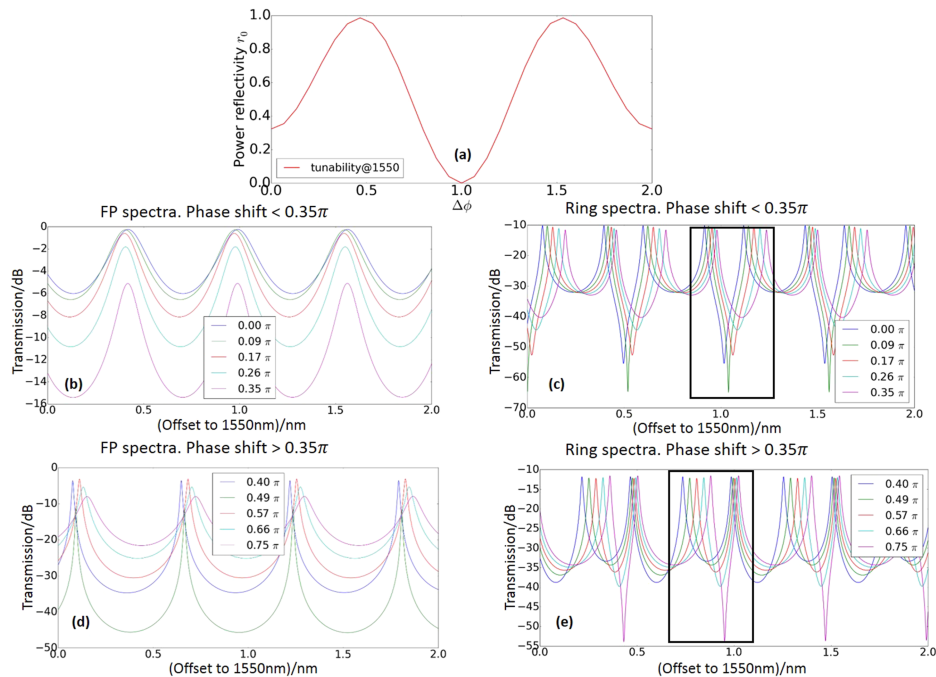


FIG. 2. Simulated tunability of our reflector (a), spectra of the embedded Fabry-Perot cavity (b) and (d), and the complete device (c) and (e). In (c) and (e), we observe that the two peaks of a split resonance may shift at different rates. This phenomenon agrees well with the former literature.¹³

Photonics.¹⁶ As clearly shown in Figs. 2(b) and 2(d), by introducing different phase shifts to the reflectors to change their reflectivities, the Fabry-Perot mode can be tuned from quite sharp (high Q) to very smooth (low Q). The smooth mode can interfere with the discrete ring resonance mode to generate the Fano resonance, as exhibited in Figs. 2(c) and 2(e). Current ring resonance mode shows a resonance splitting due to the internal reflections inside the ring cavity which couple the clockwise circulating mode and counter-clockwise circulating mode and break their degeneracy.¹⁷ Both figures indicate that in order to get a larger ER of the Fano resonance, the Q of the FP mode needs to be low which agrees well with the fundamental theory. In these two simulations, we only tune one of those reflectors with another one fixed at specific reflection for simple demonstration, while in reality both reflectors can be controlled independently.

Note that the two peaks of the split resonance shift at slightly different rates. This phenomenon agrees well with our former observations.¹³ This can be explained by two effects that are happening simultaneously. Injecting power into the phase shifter of the reflector will add an increment to the total optical length of the ring, leading to a red shift of the whole spectrum. At the same time, it will increase the reflectivity of the reflector, thus increasing the split distance of the two peaks, which means one peak will be pushed towards the longer wavelength, while the other will be pushed towards the shorter wavelength. These two effects will add up at one peak but cancel out at another peak.

The two reflectors contain balanced MZIs to provide relatively flat spectra.¹⁵ The armlength is chosen to be $200\ \mu\text{m}$ to guarantee enough phase shift. So the complete ring resonator has a very long roundtrip which leads to a small *free spectral range* (FSR). However, the armlengths of the reflectors can be further optimized down to $100\ \mu\text{m}$ or even shorter with more efficient heaters.

We also investigate how the power coupling coefficient of the ring resonator will influence the Fano resonance as shown in Fig. 3. The ER can be increased by decreasing the power coupling coefficient (thus increasing the Q factor of the ring resonator), but this comes at the price of higher insertion loss.

The microscopic figures of our devices are given in Fig. 4. The device is fabricated on IMEC's passive silicon photonics platform through the Europractice MPW service.¹⁸ The substrate is a $220\ \text{nm}$ thick SOI wafer. We design the waveguide cross section to be $450\ \text{nm} \times 220\ \text{nm}$ to ensure single mode operation. Grating couplers are employed to achieve vertical coupling between the fibers and our chip. The structures are covered by a planarized silicon dioxide protection layer, on top of which our metal heaters are processed in-house. The heaters are based on titanium resistive elements with a $2\ \mu\text{m}$ width and $100\ \text{nm}$ thickness connected with gold contact electrodes.

In Fig. 5 we plot the measurement data of our device. Similar to the simulations, we fix one reflector and sweep the power injected to the other reflector. These measurements show the same resonance shapes and shift patterns as the simulation results in Figs. 2(c) and 2(e). Due to the disperse behavior of the directional couplers, which means that the coupling coefficients vary with wavelength, the measured resonances show different extinction ratios. The maximum ER can be over $40\ \text{dB}$ within a $100\ \text{pm}$ wavelength range, which gives a sharp slope with a rate over $400\ \text{dB/nm}$, while the maximum slope rate observed at some resonances can be over $700\ \text{dB/nm}$ with an extinction ratio larger than

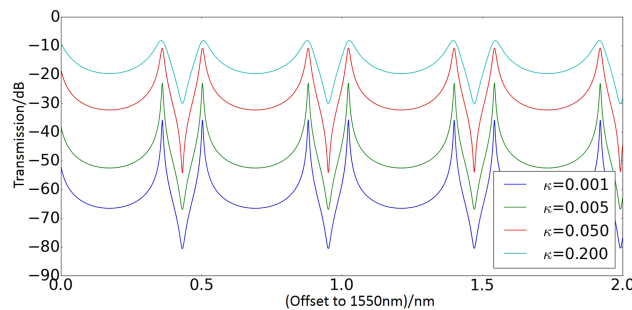


FIG. 3. Simulation shows the influence of the power coupling coefficient of the ring resonator on the performance of the Fano resonance.

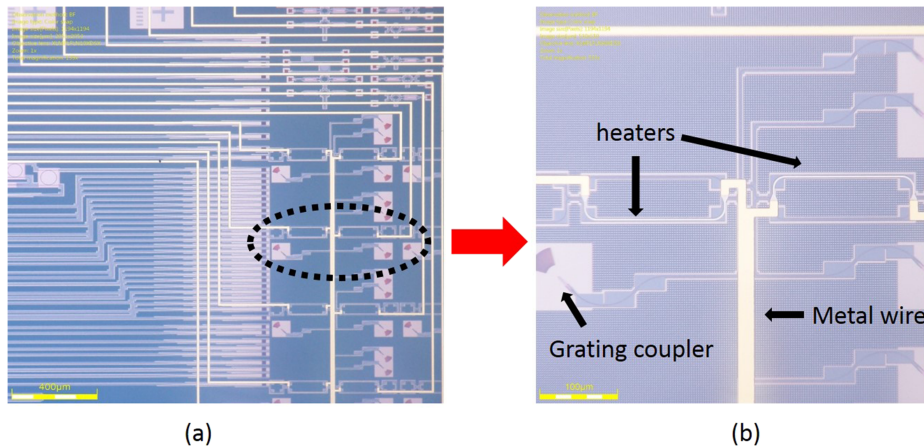


FIG. 4. Microscopic image of our devices (a) and a zoomed view of the heaters (b).

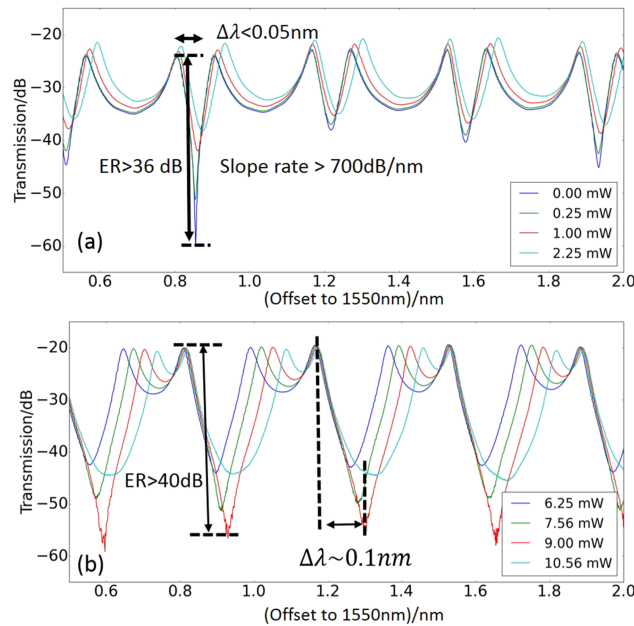


FIG. 5. Experimental measurements of the fabricated device under different power injections (a) and (b). Both exhibit the resonance shapes and shift patterns predicted by the simulations. The maximum ER can be larger than 40 dB with a corresponding slope rate over 400 dB/nm. While at other resonance, we observe an even sharper slope rate, which is over 700 dB/nm.

36 dB. As for the tuning efficiency, less than 3 mW can tune the ER to reach its maximum. The tuning of the ER is always accompanied by the shift of the wavelength, but this problem can be easily solved with an extra heater to control the ring resonance.

To summarize, we demonstrated, both in simulation and experiment, a fully integrated tunable ring resonator circuit that can generate a Fano resonance with a very high extinction ratio and slope rate. This performance will further improve Fano resonance based optical sensors, optical switches, and modulators.

¹ U. Fano, *Phys. Rev.* **124**, 1866 (1961).

² B. Luk'yanchuk, N. I. Zheludev, S. A. Maier, N. J. Halas, P. Nordlander, H. Giessen, and C. T. Chong, *Nat. Mater.* **9**, 707 (2010).

³ J.-H. Wu, J.-Y. Gao, J.-H. Xu, L. Silvestri, M. Artoni, G. C. La Rocca, and F. Bassani, *Phys. Rev. Lett.* **95**, 057401 (2005).

⁴ L. Y. Mario, S. Darmawan, and M. K. Chin, *Opt. Express* **14**, 12770 (2006).

⁵ Y. Yu, W. Xue, E. Semenova, K. Yvind, and J. Mork, *Nat. Photonics* **11**, 81 (2016).

- ⁶ F. Hao, Y. Sonnefraud, P. V. Dorpe, S. A. Maier, N. J. Halas, and P. Nordlander, *Nano Lett.* **8**, 3983 (2008).
- ⁷ G. Wang, T. Dai, J. Jiang, H. Yu, Y. Hao, Y. Wang, Y. Li, X. Jiang, and J. Yang, *J. Opt.* **19**, 025803 (2017).
- ⁸ C. Qiu, P. Yu, T. Hu, F. Wang, X. Jiang, and J. Yang, *Appl. Phys. Lett.* **101**, 021110 (2012).
- ⁹ B.-B. Li, Y.-F. Xiao, C.-L. Zou, X.-F. Jiang, Y.-C. Liu, F.-W. Sun, Y. Li, and Q. Gong, *Appl. Phys. Lett.* **100**, 021108 (2012).
- ¹⁰ W. Zhang, W. Li, and J. Yao, *Optics Lett.* **41**, 2474 (2016).
- ¹¹ G. Zhao, T. Zhao, H. Xiao, Z. Liu, G. Liu, J. Yang, Z. Ren, J. Bai, and Y. Tian, *Opt. Express* **24**, 20187 (2016).
- ¹² T. Hu, P. Yu, C. Qiu, H. Qiu, F. Wang, M. Yang, X. Jiang, H. Yu, and J. Yang, *Appl. Phys. Lett.* **102**, 011112 (2013).
- ¹³ A. Li and W. Bogaerts, *Opt. Express* **25**, 2092 (2017).
- ¹⁴ S. Fan, *Appl. Phys. Lett.* **80**, 908 (2002).
- ¹⁵ A. Li, Q. Huang, and W. Bogaerts, *Photonics Res.* **4**, 84 (2016).
- ¹⁶ M. Fiers, T. Van Vaerenbergh, K. Caluwaerts, D. V. Ginste, B. Schrauwen, J. Dambre, and P. Bienstman, *J. Opt. Soc. Am. B* **29**, 896 (2012).
- ¹⁷ A. Li, T. Vaerenbergh, P. Heyn, P. Bienstman, and W. Bogaerts, *Laser Photonics Rev.* **10**, 420 (2016).
- ¹⁸ P. Dumon, W. Bogaerts, R. Baets, J.-M. Fedeli, and L. Fulbert, *Electron. Lett.* **45**, 581 (2009).